Granular Matter (2016) 18:11
DOI 10.1007/s10035-016-0604-6

ORIGINAL PAPER

# Enhanced run-out of dam-break granular flows caused by initial fluidization and initial material expansion

**S. Montserrat**[1] · **A. Tamburrino**[1,2] · **O. Roche**[3] · **Y. Niño**[1,2] · **C. F. Ihle**[1,4]

Received: 26 March 2015 / Published online: 26 February 2016


**Abstract** We report results of the run-out of experimental dam-break flows in a horizontal channel generated from the collapse of columns of fine (75 μm) particles fluidized at various degrees. We find that the flow run-out ($x$) made dimensionless by the initial column length ($x_o$) is a power function of the initial column height-to-length ratio ($r$), as shown in previous works with non-fluidized flows. The run-out of flows initially fluidized at different degrees is accounted by $x/x_o = \alpha r^n$. For initially non-fluidized flows, our values of $\alpha$ are significantly higher than those reported earlier for flows of coarser granular material (>0.15 mm), showing that finely grained flows have longer run-outs compared to their coarser counterparts. The coefficient $\alpha$ is a function of the initial degree of fluidization, with a higher growth above 93 % of fluidization, which coincides with the onset of bed expansion, and it accounts for a flow run-out increase being up to more than twice that of non-fluidized flows. The parameter $\alpha$ is well correlated with the amount of initial bed expansion, which undergoes a sharp transition at high degrees of fluidization that has shown to be an important mechanism for reducing flow friction. Our results are consistent with earlier findings that showed that bed expansion significantly increases pore pressure diffusion timescales in static columns, suggesting that the long run-out of initially expanded finely grained flows is due to their ability to diffuse pore pressure slowly.

**Keywords** Granular flow · Run-out · Fluidization · Pore pressure · Dam-break · Experiments

## 1 Introduction

Dense geophysical gravitational flows commonly consist of fluid-particle mixtures that propagate over topography. Examples of mixtures for which the interstitial fluid phase has a non-negligible influence on flow dynamics include debris flows, lahars, pyroclastic flows and snow avalanches. Run-outs of geophysical granular flows have been observed to be larger than expected from sliding block models. Commonly predicted apparent friction angles are lower than the material repose angle or normally accepted values for geological materials [1–3]. Such friction reduction has been attributed to various mechanisms, including the presence of a basal lubrication layer formed by trapped water or air [4] or basal melting [3,5], interstitial pore-fluid pressure that causes fluidization [6–8], viscous shear reduction by random fluctuating energy [9,10], acoustic fluidization [11], flow-induced segregation effects [12–15], frictional weakening at increasing sliding velocity [16], or the dependence of the friction coefficient with the local value of gravity [3,17].

The interstitial fluid may play an important role in enhancing flow run-out as excess pore fluid pressure (i.e. greater than hydrostatic pressure) can modulate the frictional stress between the particles according to the Coulomb yield criterion [6]:

✉ S. Montserrat
smontser@ing.uchile.cl

O. Roche
o.roche@opgc.univ-bpclermont.fr

1 Advanced Mining Technology Center, Universidad de Chile, Av. Tupper 2007, Santiago, Chile

2 Departamento de Ingeniería Civil, Universidad de Chile, Av. Blanco Encalada 2002, Santiago, Chile

3 Laboratoire Magmas et Volcans, Université Blaise Pascal-CNRS-IRD, OPGC, Campus Universitaire des Cézeaux, 6 Avenue Blaise Pascal, TSA 60026 - CS 60026 Aubière Cedex, France

4 Department of Mining Engineering, Universidad de Chile, Av. Tupper 2069, Santiago, Chile

$$|\tau| = (\xi - p)\tan\phi_g + c, \quad (1)$$

where $\tau$ is the average shear stress at the yield surface, $\xi$ is the normal stress due to the particles weight, $p$ is the pore-fluid pressure, $\phi_g$ is the bulk friction angle, and $c$ is the mixture cohesion. In particular, in non-cohesive fully fluidized mixtures, $\xi = p$ and the shear stress vanishes. Excess pore fluid pressure arises in natural flows because of an interstitial upward fluid flux and/or particle settling, and it can persist through deposition [18–20]. Several field and experimental measurements have revealed the existence of excess pore-fluid pressure values well above hydrostatic levels at the base of fluid-particle flows, even at relatively long travel distances from the source [6,7,18–22], thus highlighting that long-lived excess pore pressure promotes long run-out distances even on small to horizontal slopes.

Several dam-break experiments using different granular mixtures, in both unidirectional and axisymmetric configurations, demonstrate that the dimensionless run-out of non-fluidized flows (run-out normalized by the initial column length, $x_o$) scales as a power law of the initial column height-to-length ratio, $r = h_o/x_o$ [23–27] so that

$$\frac{x}{x_o} = \alpha r^n \quad (2)$$

with $\alpha$ a constant, $n = 1$ at $r$ typically smaller than 1.5–3, and $n < 1$ for higher values of $r$ [23–27] (note that $x$ can also be normalized by the column height, $h_o$, so that $x/h_o = \alpha r^{n-1}$). An analytical solution of the Saint–Venant equations applied to granular flows at low initial column aspect ratios, typically $r < 1{-}2$, shows that the proportionality coefficient ($\alpha$) is inversely proportional to the tangent of the granular material friction angle minus the tangent of the channel slope [1,28,29]. By means of experiments at different slopes and using scaling arguments, Lube et al. [30, and references therein] extend these findings to the case of high initial column aspect ratios.

Dam-break experiments on air-particle flows fluidized at the source in an axisymmetric configuration demonstrate that the same scaling is valid [8]. However, the flow run-out is enhanced with respect to the non-fluidized counterparts (other things being equal) as internal friction is reduced by imposing initial fluidization before releasing the granular mixture, which generates a high pore-fluid pressure [7,31,32]. In other words, initial fluidization increases the values of $\alpha$. In this study, we investigate new experiments on initially fluidized granular flows on horizontal slopes in unidirectional configuration and report results on the flow run-out as a function of the initial degree of fluidization that controls material expansion. We measured the flow run-out for the whole range of initial fluidization degrees (from none to complete fluidization), thus enlarging the number of initial conditions reported by Roche et al. [7,31,33] and Roche [32]. The analysis of the flow run-out as function of initial fluidization we present here shows that the initial bed expansion, in addition to the initial degree of fluidization, accounts for much of the flow run-out. Bed expansion occurs as a consequence of fluidization and marks a phase transition within the granular bed dividing a "solid-like" state, where particles nearly maintain permanent contacts, and a "fluid-like" state where expansion increases the free path between particles reducing long-lasting contacts and increasing granular temperature [34–37].

## 2 Experimental device and procedure

The experimental device consisted of a 300 cm-long and 10 cm-wide horizontal flume connected to a 10 cm-wide head reservoir of variable length, $x_o$ (from 5 to 20 cm), equipped with a sluice gate to keep particles confined before release (Fig. 1). The entire flume was made of transparent plexiglass to permit flow visualization. Particles in the reservoir, initially at rest, could be aerated at different degrees, from none to complete fluidization, by introducing a vertical air flux through a basal 10 mm-thick porous plate featuring a mean pore size of 20 μm, which ensured homogeneous fluidization. The air was supplied by a compressor and was dried before entering a basal wind-box filled with coarse particles (3 mm in diameter) in order to reduce its volume and to homogenize the airflow. The granular bed was fully fluidized when the drag force exerted by the vertical interstitial airflow entirely supported the weight of the particles.

We used nearly spherical glass beads (Ballotini, Potters Industries), with a density $\rho_p = 2500\ \mathrm{kg/m^3}$, a diameter $d \sim 75 \pm 15\ \mu\mathrm{m}$, and a repose angle $\phi \sim 28° \pm 1°$. These fine

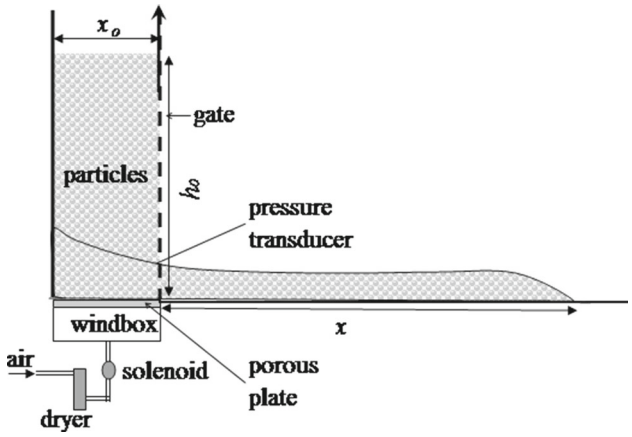


**Fig. 1** Scheme of the experimental device, consisting of a fluidization reservoir and a horizontal channel. The variables $x_o$ and $h_o$ denote the initial granular column length and non expanded height, respectively. The flow run-out normal to the reservoir gate is $x$

particles were chosen to ensure slow pore-fluid pressure diffusion owing to low material permeability ($k \sim 10^{-11}$ m$^2$). This is in contrast with beds of coarser particles (with higher permeability, as $k$ is proportional to $d^{\sim 2}$ [38]) for which diffusion is nearly instantaneous at laboratory scale and thus has little influence in collapse processes [8]. The bulk density of the granular mixture was measured and was $\rho \sim 1450$ kg/m$^3$, thus the solid volume fraction $\upsilon = 58$ %. In terms of their fluidization properties, the particles belonged to group A according to Geldart's classification [39]. This means that, nominally, beds of these particles expand homogeneously at gas velocities, $U$ (defined as the volumetric flow rate divided by reservoir horizontal area), between the minimum fluidization velocity ($Umf \sim 7$ mm/s in our case), at which the weight of the particles was counterbalanced, and the minimum bubbling velocity ($Umb \sim 12$ mm/s in our case), at which gas bubbles formed [33]. In practice, as shown hereafter, the onset of bed expansion, which can be used to define $Umf$ of a purely monodisperse material, occurs for fluidization degrees lower than complete fluidization (i.e. at $U < Umf$), while the latter is attained for gas velocities higher than $Umb$. For this reason, we prefer to account for the initial degree of fluidization by directly measuring the pore fluid pressure at the base of the granular column. In the following, Geldart's [39] group A particles will be called indistinctly as fine particles.

Both $Umf$ and $Umb$ (and their associated pore-pressures) may vary in relatively thin beds because of wall effects and airflow channeling [40–43]. However, no significant effects are observed in the fluidization properties when the bed is thicker than ~2–5 cm [41] or the ratio between the column bed length ($x_o$, or diameter in the case of a cylindrical configuration) and particle diameter ($d$) is larger than about 30 [40–43]. In our experiments $x_o/d > 1000$ ($x_o \sim 0.1$ and d $\sim 75$ μm), thus wall effects are expected to be negligible.

The basal pore fluid pressure was measured before the sluice gate opening using a piezoresistive pressure sensor (ICSensors$^{TM}$, model 145N, [7,32]) located on one side-wall of the reservoir at the lowest position. The sensor measured pressure in the range 0 to ~34.5 kPa (0–5 psi) and was placed inside an aluminum casing covered by a 38 μm-aperture grid (see [7] for detail). In order to ensure reproducibility of the experiments, particles were fluidized for one hour with dry air before running the experiments to eliminate possible mild cohesion caused by ambient moisture. During the whole procedure virtually no particle was found to attach to the walls and not any flowing clusters were observed, thus implying that no relevant static electricity effects were present during the experiment. The granular flow along the flume was generated by a rapid release of the reservoir gate (<0.1 s). When the gate was removed, the air flux was instantaneously stopped by the action of a solenoid valve connected to an electric switch activated by the gate movement. This procedure differs with that used in earlier studies for which the air flux was still present even after the gate was released (e.g. [32]), an aspect that is analyzed below. The porous plate was assumed to be an impermeable wall during the flow motion (see [44]).

## 3 Results

### 3.1 Initial fluidization and onset of bed expansion

We quantify the initial degree of fluidization at the head reservoir as $\beta o = p_o/P_L$, where $p_o$ is the measured pore fluid pressure at the base of the granular column and $P_L = \rho g h_o$ is the lithostatic pressure where $\rho$ is the bulk mixture density, $g$ is the gravity acceleration, and $h_o$ is the non-expanded column height [44]. Figure 2 shows the amount of expansion of the initial fluidized column for a range of values of the column aspect ratio, $r = h_o/x_o$, as a function of the initial degree of fluidization. Bed expansion occurs at $\beta o = \beta o_c \sim 0.93$ and increase up to $\Delta h^* = (h_e - h_o)/h_o = 0.05$, where $h_e(\beta o)$ is the expanded bed height. The bed expansion, $\Delta h^*(\beta o)$, can be estimated as:

$$\Delta h^* = 0, \quad \beta_o < \beta_{oc}, \tag{3a}$$

$$\Delta h^* = a + b\beta_o, \quad \beta_o > \beta_{oc}, \tag{3b}$$

where $a = -0.62$ and $b = 0.67$ are best fitted values of Eq. (3) to the experimental results.

### 3.2 Flow run-out

Results show that, for a given initial aspect ratio, the dimensionless flow run-out increases linearly with $\beta o$ up to a value

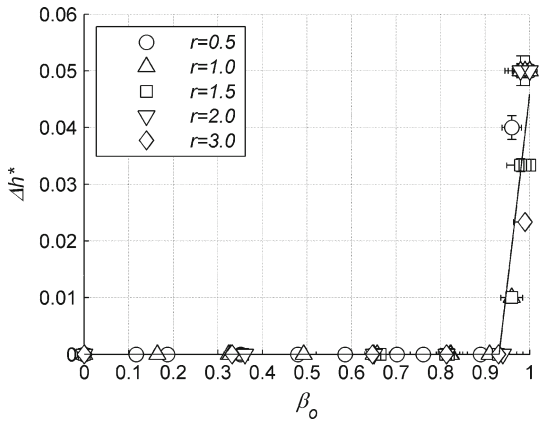


**Fig. 2** Bed expansion as a function of the dimensionless initial fluidization degree, $\beta o$, for different column aspect ratios, $r = h_o/x_o$. $\Delta h^* = (h_e - h_o)/h_o$, where $h_o$ is the initial, non expanded column height and $h_e$ is the expanded height. Expansion occurs when $\beta o > \beta o_c \sim 0.93$. The *line* corresponds to the best fit of the experimental data according to Eq. (3)

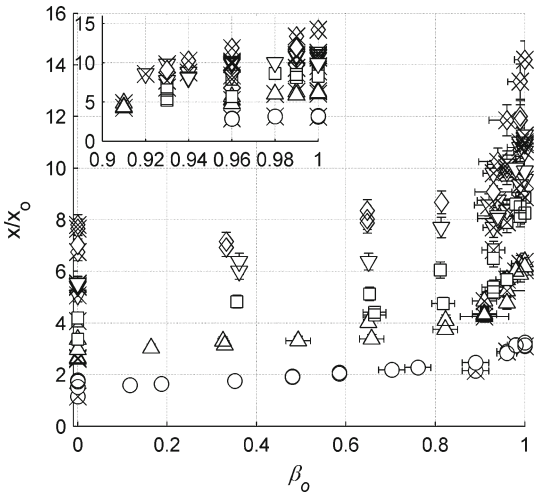


**Fig. 3** Dimensionless flow run-out, $x/x_o$ as a function of the initial degree of fluidization, $\beta o$. *Symbols* represent different aspect ratios, the same as Fig. 2. *Symbols* marked with an × corresponds to those reported by Roche et al. [31]. Note that *symbols* may be larger than error bars

of $\beta o = \sim \beta o_c$ (Fig. 3). For $\beta o > \beta o_c$, the flow run-out continues increasing with $\beta o$ but at a much higher rate. This sharp transition in the trend of the dimensionless flow runt-out with $\beta o$ at $\beta o = \beta o_c$ seems to be correlated with the transition observed on the trend of $\Delta h^*$ at the same $\beta o$-value. Despite the air flux is stopped at flow initiation in our experiments, the run-outs are close to those reported by Roche et al. [31] at $\beta o = 0$ (or $U = 0$), $\beta o \sim \beta o_c$ (or *Umf*, at the onset of bed expansion) and $\beta o > \beta o_c$ ($U > Umf$). This shows that the fluidization process at the source (i.e. continuous or stopped airflow) has not significant effects on the flow run-out and can be further explained as no air flux is provided during flow propagation in the channel. There are differences, however, in the geometry of flow deposits. Deposits resulting from continuous fluidization at the source first show a flat horizontal surface at the reservoir, and exhibit a decreasing thickness profile that is maximum at the entrance of the channel (cf. [7,31]). In contrast, when the air flux causing fluidization is stopped at flow initiation, the thickness monotonically decreases downstream and the deposit takes the form of a slender wedge (Fig. 4). In spite of this slight difference, as the flow run-outs in this study are comparable to those reported by Roche et al. [31], we merge their data with our data set to obtain more reliable results.

### 3.2.1 Run-out of non-fluidized flows

Following Mangeney et al. [45] and Lube et al. [30], the dimensionless run-out of non-fluidized flows (i.e. $\beta o = 0$) can be expressed as:

$$\frac{x_d(r)}{x_o} = \alpha_L r \pm \sigma_d, \quad r < r_t, \tag{4a}$$

$$\frac{x_d(r)}{x_o} = \alpha_H r^n \pm \sigma_d, \quad r > r_t, \tag{4b}$$

where $x_d(r)$ is the run-out of non-fluidized flows for a given initial column aspect ratio $(r)$, $\alpha_L$ and $\alpha_H$ are proportionality constants for low and high initial column aspect ratios, respectively, $n$ is an exponent (lower than but close to 1) fit to the experimental results, $r_t$ is a transition aspect ratio typically in the range 1.5–3, and $\sigma_d$ is the corresponding experimental error estimated here as the standard deviations of the data [6,23,25]. In order to determine $\alpha_L$, $\alpha_H$ and $n$ we fitted Eqs. (4a)–(4b) to our experimental results, and obtained $\alpha_L = 2.81$, $\alpha_H = 3.03$, $n = 0.80$, $r_t = 1.46$ and $\sigma_d = 0.31$ (Fig. 5a). A good collapse of the flow run-out data is observed for $r$-values ranging from 0.4 to 4.

The flow run-out can be also normalized by the initial column height, $h_o$, instead of $x_o$ [7,8,31], so that:

$$\frac{x_d(r)}{h_o} = \alpha_L \pm \sigma_{dh}, \quad r < r_t, \tag{5a}$$

$$\frac{x_d(r)}{h_o} = \alpha_H r^{n-1} \pm \sigma_{dh}, \quad r > r_t, \tag{5b}$$

where $\sigma_{dh}$ represents the error for $x_d/h_o$, estimated by propagating individual experimental errors and assuming that the error for $x_d/x_o$ is $\sigma_d$:

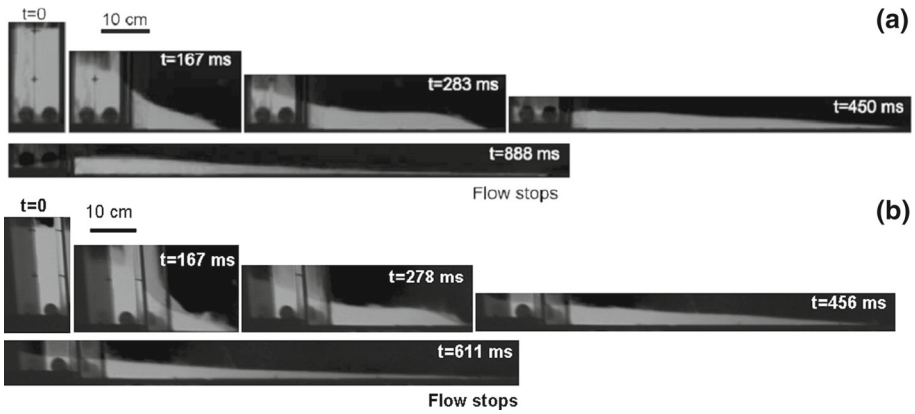


**Fig. 4** Snapshot of dam-break flows (time in milliseconds). Flows generated from columns ($h_o = 20$ cm and $x_o = 10$) of granular material. **a** Continually fluidized at source during the whole flow emplacement [31] and **b** whose fluidization is stopped at flow initiation, this study

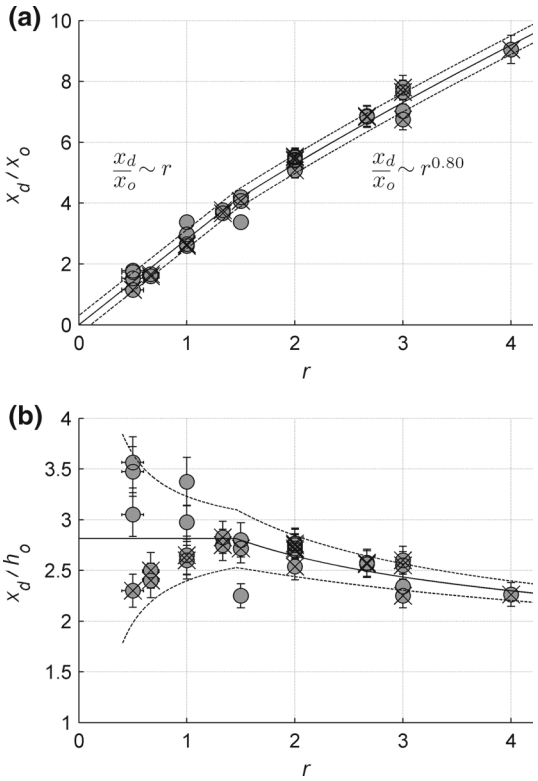


**Fig. 5** **a** Dimensionless run-out of non-fluidized flows (i.e. $\beta o = 0$) normalized by the initial column length, $x_o$, as a function of the initial column aspect ratio, $r$. Fitted values for parameters of Eqs. (4a)–(4b) are $\alpha_L = 2.81$, $\alpha_H = 3.03$ and $n = 0.80$. The *line* represent the solution of Eq. 4 while *dashed lines* denote the standard deviation of the data $\pm\sigma_d$. **b** Run-out of non-fluidized flows (i.e. $\beta o = 0$) normalized by the initial column height, $h_o$. The *line* represents the solution of Eq. (5) while *dashed lines* represent data dispersion according to Eq. (6). *Symbols* marked with an $\times$ corresponds to those reported by Roche et al. [31]. Note that *symbols* may be larger than *error bars*

$$\sigma_{dh} = \sqrt{\left(\frac{\sigma_d}{r}\right)^2 + \left(\frac{x_d/x_o}{r^2} e_r\right)^2}, \tag{6}$$

In Eq. (6), $e_r$ represents the experimental error of $r$. As shown by Eq. (5a), for low initial column aspect ratio $x_d/h_o = \alpha_L$ is constant. However, as $\sigma_{dh} \sim \sigma_d/r$, there is higher data dispersion for $r < r_t$, as shown in Fig. 5b. A good fit of the data, however, is observed at high initial aspect ratios, $r > r_t$. This may partly explain while $x_o$ instead of $h_o$ has been generally preferred for presenting the normalized run-out data of dam-break granular flows.

### 3.2.2 Run-out of initially fluidized flows

For a given initial column geometry (i.e. same $x_o$ and $h_o$), the increase in run-out due to the initial fluidization in comparison with non-fluidized flows can be simply estimated as $\alpha_f \equiv x/x_d$ (Fig. 6), with the variables $x$ and $x_d$ corresponding to the run-out of fluidized or non-fluidized

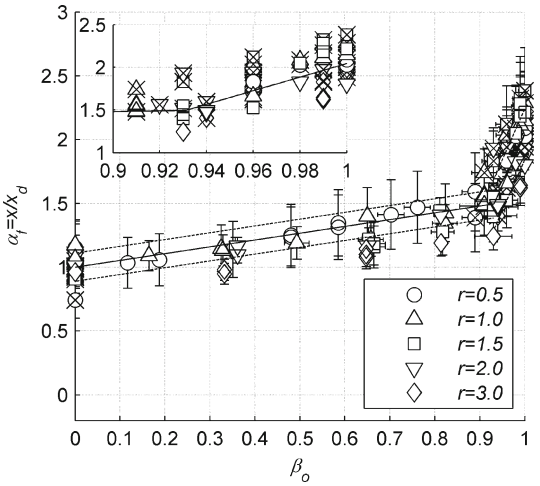


**Fig. 6** Flow run-out, $x$, normalized by the run-out of non-fluidized mixtures, $x_d$ (at $\beta o = 0$), as a function of the initial degree of fluidization, $\beta o$. The *solid lines* represent the best fit obtained from Eq. 7, while *dashed lines* denote the standard deviation of experimental data ($\pm\sigma\alpha_{1,2}$). *Symbols* marked with an $\times$ correspond to those reported by Roche et al. [31]. Note that *symbols* may be larger than *error bars*

flows, respectively. Thus, the parameter $\alpha$ in Eq. (2) can be expressed as $\alpha = \alpha_f \alpha_L$ for $r < r_t$ and $\alpha = \alpha_f \alpha_H$ for $r > r_t$. Interestingly, values of $\alpha_f$ at different aspect ratios collapse on a single curve as a function of $\beta o$. Although $\alpha_f$ is independent on $r$ at $\beta o = 0$, for high values of $r$ and $\beta o > 0$ there could be a weak dependence of $\alpha_f$ with $r$ as $\alpha_f$ shows to be systematically below the fitted tendency in Fig. 6. $\alpha_f$ varies linearly with $\beta o$, until it increases abruptly at $\beta o = \beta o_c$, which coincides with the onset of bed expansion. Fitting $x/x_d \equiv \alpha_f$ as a piecewise linear function of $\beta o$ and $\Delta h^*$, and imposing the condition $\alpha_f(\beta o = 0) = 1$, the normalized run-out can be estimated as

$$\frac{x}{x_d} = \alpha_f = \left(1 + m_1 \beta_o + m_2 \Delta h^*\right) \pm \sigma_{\alpha 1,2}, \tag{7}$$

where $m_1$ and $m_2$ are the slopes of the straight lines fitting the data, $\sigma_{\alpha 1}$ and $\sigma_{\alpha 2}$ are the corresponding experimental errors estimated here as the standard deviations of the data for $\beta o < \beta o_c$ and $\beta o > \beta o_c$, respectively, and $\Delta h^*(\beta o)$ is estimated according to Eq. (3). The values of the constants $m_1$ and $m_2$ are those that minimize the root mean square value of the data dispersion of Eq. (7), so that $m_1 = 0.53$, $m_2 = 11.12$, $\sigma_{\alpha 1} = 0.11$ and $\sigma_{\alpha 2} = 0.20$. Figure 6 shows that $\alpha_f$ increases from 1 to 1.50 in the range $0 < \beta o < \beta o_c$, and then increases abruptly up to $2 \pm 0.5$ when $\beta o = 1$. As $\Delta h^*$ is a sole function of $\beta o$ (Eq. 3), the large value of $m_2$ compared to $m_1$ shows that the increase in run-out (respect to non-fluidized flows) at $\beta o > \beta o_c$ is caused mainly by initial bed expansion and not only the initial degree of fluidization (cf. [46]).

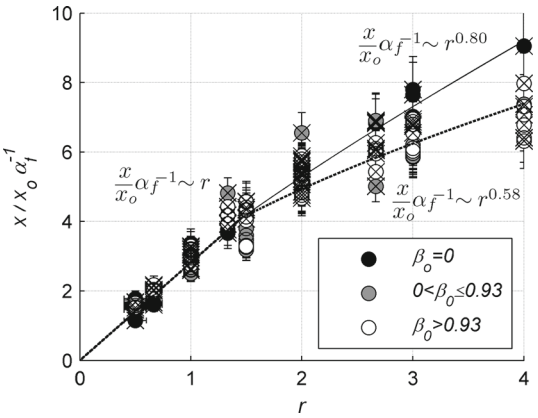


**Fig. 7** Dimensionless run-out of initially fluidized or non-fluidized flows, $x/x_o$, rescaled by $\alpha_f$, as a function of the initial column aspect ratio, $r$. The *continuous line* represents the solution of Eqs. 7a–b for initially non-fluidized flows ($\beta o = 0$) while the *dashed lines* corresponds to the solution for the same equation but for flows initially fluidized at different degrees ($\beta o > 0$). *Symbols* marked with an × correspond to those reported by Roche et al. [31]. Note that *symbols* may be larger than *error bars*

Combining Eqs. (4a)–(4b) and (7), the flow run-out of initially fluidized or non-fluidized flows, $x$, normalized by $x_o$ can be expressed as:

$$\frac{x}{x_o} = \alpha_f \alpha_L r, \quad r < r_t, \tag{8a}$$

$$\frac{x}{x_o} = \alpha_f \alpha_H r^n, \quad r > r_t. \tag{8b}$$

Equations (8a)–(8b) are an extension of Eqs. (4a)–(4b) for non-fluidized flows, which are recovered if $\beta o = 0$ and $\alpha_f = 1$. For $r < r_t$, the rescaled flow run-out, $x/x_o\alpha_f^{-1}$, where $\alpha_f$ includes the effect of fluidization on the flow run-out, follows the same tendency observed for non-fluidized flows (Fig. 7, compare with Fig. 5a) and is independent of the initial degree of fluidization ($\beta o$). We stress that in this range of $r$-values no systematic variation of the normalized run-out with $\beta o$ was observed at a given value of $r$. The data dispersion is in accordance with the estimated experimental error of the rescaled dimensionless flow run-out, with maximum absolute values near $\pm 1$. This experimental error results from propagating individual errors of the experimental measurements ($x_f$ and $x_o$) and the error associated with $\alpha_f$ assumed to be equal to $\pm\sigma_{\alpha 1,2}$ (Eq. 7). For $r > r_t$, the tendency of the rescaled flow run-out deviates from that of non-fluidized flows at $\beta o = 0$ for which $n = 0.80$ (Fig. 7). The deviation is accounted by a reduction of the exponent $n$ due to fluidization, so that $n = 0.58$ for $\beta o > 0$ (note a relatively large dispersion of the data). We stress that there is no significant variation in the value of $n$ for the different ranges of $\beta o$, either below or above $\beta o_c$.

## 4 Discussion

### 4.1 Scaling law parameters

In our experiments, the transition of scaling laws between low and high column aspect ratios occurs at $r_t \sim 1.5$, similar to the value reported in earlier studies using both unidirectional or axisymmetric configurations (e.g. [6,8,23,25]). For any degree of fluidization, our results reveal a linear dependency of the dimensionless run-out with $r$ at $r < r_t$, as shown by Roche et al. [8] for initially fluidized flows in the axisymmetric configuration, for which lateral spreading has negligible influence on $n$ at such low $r$ values. However, for non-fluidized flows and at high values of $r > \sim 1.5$, the fitted value $n = 0.80$ ( Fig. 7) is larger than that for similar unidirectional flows but of coarser (>0.15 mm) particles ($n = \sim 0.67$) [26,30], which means that the run-out of non-fluidized flows of fine particles increases respect to $r$ at a higher rate compared with their coarser counterparts. In contrary, for initially (partially) fluidized flows $n$ drops to a value of $n = 0.58$.

Comparing different studies of non-fluidized granular collapses in channels, Roche et al. [8] noticed that at high $r$, $n$ approaches 1 as the channel width increases, suggesting that the reduction in the value of $n$ can be caused by sidewall effects. This can explain the larger values of $n$ in our experiments on non-fluidized flows of fines compared to similar flows of coarse particles because sidewall effects should be correlated with the channel width to particle size ratio so that the higher is the value of this ratio, the smaller are side-walls effects.

The effect of initial fluidization in reducing $n$-values is not so clear. The increase in flow run-out due to the initial degree of fluidization ($\beta o$) follows significant different trends depending if $\beta o < \beta o_c$ or $\beta o > \beta o_c$. However, for $\beta o > 0$, $n$ is independent of the initial degree of fluidization. Results suggest that $n$ presents a sharp transition at $\beta o > 0$, but the mechanism behind this transition is not clear. Following the above analysis it is clear that $n$ depends on particle size and whether these are initially (partially) fluidized or not.

Our values of $\alpha_L = 2.81$ and $\alpha_H = 3.03$ (Eq. 4) for non-fluidized flows of fine particles are respectively ~80 % and ~40 % higher than those reported by Lube et al. [26,30] for similar flows but consisting of particles of different shapes and coarser than ~0.15 mm. This, however, is consistent with experiments performed by Roche et al. [8, see their Fig. 6] but in axisymmetric horizontal configuration, which showed that the run-out of flows of fines was longer than that of flows of coarser particles. These results suggest that $\alpha_L$ and $\alpha_H$ are material-dependent [8,24] and that, other things being equal, flows of fine particles have longer run-outs than flows of coarser particles. This might be explained by par-

tial auto-fluidization of the fine material when the column collapses, as proposed by Roche et al. [8] based on experimental measurements of the interstitial air pore pressure in dam-break experiments. This study revealed that up to nearly 16 % of the total weight of particles can be supported [7]. Thus, even if non-fluidized at the source, some amount of pore pressure could arise from air-particle interactions in the shearing finely grained mixtures [31,47].

### 4.2 Influence of initial fluidization and material expansion

Our results show that the proportionality parameter $\alpha$ in Eq. (2) depends on $\beta o$, which accounts for the initial degree of fluidization and bed expansion. We show that $\alpha$ can be well estimated as $\alpha = \alpha_f\ (\alpha_L, \alpha_H)$, where $\alpha_L$ and $\alpha_H$ are the $\alpha$-constant estimated for non-fluidized flows, for low and high initial aspect ratios respectively, and $\alpha_f$ is a function of $\beta o$ accounting for the increase in flow run-out due to the initial degree of fluidization (Fig. 6). The weak dependence of $\alpha_f$ with $r$, observed for high values of $r$ can be explained by the observed reduction in the parameter $n$ due to the initial degree of fluidization, as discussed above. We note that we cannot conclude about the dependency of $\alpha_f$ upon different fine particles (type-A particles according to Geldrat [39]), as we used just one material with a given mean grain size. The flow run-out increases by 50 % when $\beta o$ varies from 0 to $\beta o_c$, while it is nearly 2–2.5 times greater than that of non-fluidized flows at $\beta o = 1$. This result shows that the major increase in flow run-out occurs in a narrow range of fluidization degrees where material expansion is observed (at $\beta o > \beta o_c$, Figs. 2, 6). Our data are consistent with those of Girolami et al. [46,48,49] who reported an important increase in run-out of volcanic ash flows when the material was expanded by initial fluidization.

Bed expansion, in addition to the effect of pore pressure that reduces flow friction according to the Coulomb yield criterion (Eq. 1), it increases the free path between particles thus reducing interparticle long-lasting contacts. Coincidentally, increasing granular temperature has been observed in fine granular beds (of type-A particles according to Geldart [39]) for fluidization degrees to cause bed expansion [34,36]. It has been observed in experimental and numerical studies that the increase in voidage (or expansion) results in an important drop of friction in fluidized columns as well as sheared flows [34–37]. This is clearly reflected in Eq. (7). The pure effect of fluidization in the increasing run-out, $\alpha_f$, is continuous and varies linearly with $\beta o$ (second term at the right hand side of Eq. 7), according to the Coulomb yield criterion (Eq. 1). However, the effect of bed expansion (third term at the right hand side of Eq. 7) causes a discontinuous jump at $\beta o = \beta o_c$, which could be interpreted as a first order phase transition occurring at the onset of bed expansion.

The increase in flow run-out with the material expansion can be also correlated with the increase in pore pressure diffusion timescales as measured in static beds [44]. Pore pressure diffusion can be modeled as a linear diffusion equation. In one spatial dimension [44, and references therein]:

$$\frac{\partial p}{\partial t} = D\frac{\partial^2 p}{\partial z^2} \tag{9}$$

where $p$ is pore pressure, $t$ is time, $z$ the vertical coordinate and $D$ the diffusion coefficient. Thus, for a constant value of $D$, the greater the initial degree of fluidization the longer is the time required to diffuse away the total excess pore pressure, explaining the increase in the flow run-out for $\beta o < \beta o_c$. The abrupt increases in $\alpha_f$ for $\beta o > \beta o_c$ coincides with the onset of material expansion. For fine particles similar to those considered in this study (see Figure 4 in [44]) Montserrat et al. [44] reported an abrupt drop of the coefficient $D$ for $\beta o > \beta o_c$, and thus an abrupt increase in the diffusion timescale. In poorly drained materials with low hydraulic permeability (i.e. finely grained mixtures) pore pressure can arise via pore volume compaction due to the consolidation of the granular network [19,20,50]. Thus, the reduction in the pore pressure diffusion coefficient, $D$, observed for initially expanded columns, can be explained by the competing processes of pore pressure generation due to mixture consolidation and of pore pressure decrease through diffusion [19,20,44].

## 5 Conclusions

Our study focused on the run-out of air-particle mixture flows using a lock-exchange flume. The data revealed that the run-out of flows of fine (75 μm) particles increased with the initial material expansion controlled by the degree of fluidization. Our results show that (i) the dimensionless flow run-out, $x/x_o$ , scales as a power law of the initial column height-to-length ratio, $r = h_o/x_o$, as reported in earlier studies on non-fluidized unidirectional flows of coarse particles [26,30]; (ii) the exponent $n$ of the power law depends on particle size and whether particles are fluidized at different degrees or not ($n = 0.80$ for $\beta o = 0$ and $n = 0.58$ for $\beta o > 0$), extending the finding by Roche et al. [8] in axisymmetric configuration; and (iii) the proportionality parameter in Eq. (2), $\alpha$, is strongly dependent on $\beta o$ and the amount of bed expansion.

We show that $\alpha$ can be expressed as $\alpha = \alpha_f\ (\alpha_L, \alpha_H)$, with $\alpha_f$ a sole function of $\beta o$ that accounts for a mobility increase due to the initial degree of fluidization. The constants $\alpha_L$ and $\alpha_H$ have been obtained for non-fluidized flows at low and high initial aspect ratios, respectively. The parameter $\alpha_f$ is a piecewise linear function of the initial degree

of fluidization and bed expansion, with a marked increase above $\beta oc \sim 0.93$, which coincides with the onset of bed expansion. The increase of the parameter $\alpha_f$, and thus of the flow run-out, with the initial degree of fluidization can be explained by two mechanisms. The first is the increase of pore pressure diffusion timescales as shown in studies on static columns (see Figure 6 in [44]), as $\alpha_f$ increases linearly with the initial degree of fluidization, with an abrupt change in tendency for $\beta o > \beta o_c$. The abrupt increase in run-out for $\beta o > \beta o_c$ coincides with an abrupt drop in pore pressure diffusion coefficients, $D$, and thus an increase in pore pressure diffusion time scales due to initial material expansion [44]. The second mechanism is low friction in fluidized granular beds as well as in shearing granular flows that is due to voidage increase caused by the material expansion.

**Acknowledgments** This work was supported by ECOS-CONICYT Project C11U01, Institut de Recherche pour le Développement (IRD, France), Departamento de Ingeniería Civil, Universidad de Chile, Advanced Mining Technology Center (AMTC) and the Chilean National Commission for Scientific and Technological Research, CONICYT, through Fondecyt Projects Nos. 11110201, 11130254 and 1130910. K. Hutter and an anonymous reviewer are thanked for fruitful reviews. This is Laboratory of Excellence *ClercVolc* contribution no. 189.

## References

1. Lucas, A., Mangeney, A.: Mobility and topographic effects for large Valles Marineris landslides on Mars. Geophys. Res. Lett. **34**, L10201 (2007)
2. Pirulli, M., Mangeney, A.: Results of back-analysis of the propagation of rock avalanches as a function of the assumed rheology. Rock Mech. Rock Eng. **41**(1), 59–84 (2008)
3. Singer, K.N., McKinnon, W.B., Schenk, P.M., Moore, J.M.: Massive ice avalanches on Iapetus mobilized by friction reduction during flash heating. Nat. Geosci. **5**, 574–578 (2012)
4. Shreve, R.L.: Leakage and fluidization in air-layer lubricated avalanches. Geol. Soc. Am. Bull. **79**, 653–658 (1968)
5. Goren, L., Aharonov, E.: Long runout landslides: the role of frictional heating and hydraulic diffusivity. Geophys. Res. Lett. **34**, L07301 (2007)
6. Iverson, R.M.: The physics of debris flows. Rev. Geophys. **35**, 245–296 (1997)
7. Roche, O., Montserrat, S., Niño, Y., Tamburrino, A.: Pore fluid pressure and internal kinematics of gravitational laboratory air-particle flows: insights into the emplacement dynamics of pyroclastic flows. J. Geophys. Res. **115**, B09206 (2010)
8. Roche, O., Attali, M., Mangeney, A., Lucas, A.: On the run-out distance of geophysical gravitational flows: insight from fluidized granular collapse experiments. Earth Planet. Sci. Lett. **311**, 375–385 (2011)
9. Bartelt, P., Buser, O., Platzer, K.: Fluctuation dissipation relations for granular snow avalanches. J. Glaciol. **52**(179), 631–643 (2006)
10. Bartelt, P., Buser, O., Platzer, K: Starving avalanches: frictional mechanisms at the tails of finite- sized mass movements. Geophys. Res. Lett. **34**, L20407 (2007)
11. Collins, G.S., Melosh, H.J.: Acoustic fluidization and the extraordinary mobility of sturzstroms. J. Geophys. Res. **108**(B10), 2473 (2003)
12. Linares-Guerrero, E., Goujon, C., Zenit, R.: Increased mobility of bidisperse granular avalanches. J. Fluid Mech. **593**(1), 475–504 (2007)
13. Roche, O., Gilbertson, M.A., Phillips, J.C., Sparks, R.S.J.: The influence of particle size on the flow of initially fluidised powders. Powder Technol. **166**(3), 167–174 (2006)
14. Phillips, J.C., Hogg, A.J., Kerswell, R.R., Thomas, N.H.: Enhanced mobility of granular mixtures of fine and coarse particles. Earth Planet. Sci. Lett. **246**(3), 466–480 (2006)
15. Meruane, C., Tamburrino, A., Roche, O.: Dynamics of dense granular flows of small-and-large-grain mixtures in an ambient fluid. Phys. Rev E **86**(2), 026311 (2012)
16. Lucas, A., Mangeney, A., Ampuero, J. P.: Frictional velocity-weakening in landslides on Earth and on other planetary bodies. Nat. Commun. **5**, 3417 (2014)
17. Kleinhans, M.G., Markies, H., de Vet, S.J., Postema, F.N.: Static and dynamic angles of repose in loose granular materials under reduced gravity. J. Geophys. Res. **116**, E11004 (2011)
18. Major, J.J., Iverson, R.M.: Debris-flow deposition: effects of pore-fluid pressure and friction concentrated at flow margins. Geol. Soc. Am. Bull. **111**, 1424–1434 (1999)
19. Major, J.J.: Gravity-driven consolidation of granular slurries—implications for debris-flow deposition and deposit characteristics. J. Sedim Res. **70**, 64–83 (2000)
20. Goren, L., Aharonov, E., Sparks, D., Toussaint, R.: Pore pressure evolution in deforming granular material: a general formulation and the infinitely stiff approximation. J. Geophys. Res. **115**, B09216 (2010)
21. McArdell, B.W., Bartelt, P., Kowalski, J.: Field observations of basal forces and fluid pore pressure in a debris flow. Geophys. Res. Lett. **34**, L07406 (2007)
22. Iverson, R.M., Logan, M., LaHusen, R.G., Berti, M.: The perfect debris flow? Aggregated results from 28 large-scale experiments. J. Geophys. Res. **115**, F03005 (2010)
23. Lajeunesse, E., Mangeney, A., Vilotte, J.P.: Spreading of a granular mass on a horizontal plane. Phys. Fluids **16**, 2371 (2004)
24. Balmforth, N.J., Kerswell, R.R.: Granular collapse in two dimensions. J. Fluid Mech. **538**, 399–428 (2005)
25. Lube, G., Huppert, H.E., Sparks, R.S.J., Hallworth, M.A.: Axisymmetric collapses of granular columns. J. Fluid Mech. **508**, 175–199 (2004)
26. Lube, G., Huppert, H.E., Sparks, R.S.J., Freundt, A.: Collapses of two-dimensional granular columns. Phys. Rev. E. **72**, 041301 (2005)
27. Lajeunesse, E., Monnier, J.B., Homsy, G.M.: Granular slumping on a horizontal surface. Phys. Fluids **17**, 103302 (2005)
28. Mangeney-Castelnau, A., Bouchut, F., Vilotte, J.P., Lajeunesse, E., Aubertin, A., Pirulli, M.: On the use of Saint Venant equations to simulate the spreading of a granular mass. J. Geophys. Res. **110**, B09103 (2005)
29. Mangeney, A., Roche, O., Hungr, O., Mangold, N., Faccanoni, G., Lucas, A.: Erosion and mobility in granular collapse over sloping beds. J. Geophys. Res. **115**, F03040 (2010)
30. Lube, G., Huppert, H.E., Sparks, R.S.J., Freundt, A.: Granular column collapses down rough, inclined channels. J. Fluid Mech. **675**, 347–368 (2011)
31. Roche, O., Montserrat, S., Niño, Y., Tamburrino, A.: Experimental observations of water-like behavior of initially fluidized, dam break granular flows and their relevance for the propagation of ash-rich pyroclastic flows. J. Geophys. Res. **113**, B12203 (2008)
32. Roche, O.: Depositional processes and gas pore pressure in pyroclastic flows: an experimental perspective. Bull. Volcanol. **74**, 1807–1820 (2012)
33. Roche, O., Gilbertson, M., Phillips, J.C., Sparks, R.S.J.: Experimental study of gas-fluidized granular flows with implications

for pyroclastic flow emplacement. J. Geophys. Res. **109**, B10201 (2004)
34. Cody, G.D., Goldfarb, D.J., Storch Jr., G.V., Norris, A.N.: Particle granular temperature in gas fluidized beds. Powder Technol. **87**, 211–232 (1996)
35. Aharonov, E., Sparks, D.: Rigidity phase transition in granular packings. Phys. Rev. E. **60**(6), 6890–6896 (1999)
36. Biggs, M.J., Glass, D., Xie, L., Zivkovic, V., Buts, A., Kounders, M.C.: Granular temperature in a gas fluidized bed. Granul. Matter **10**(2), 63–73 (2008)
37. Nichol, K., Zanin, A., Bastien, R., Wandersman, E., van Hecke, M.: Flow-induced agitations create a granular fluid. Phys. Rev. Lett. **104**(7), 078302 (2010)
38. Shepherd, R.G.: Correlations of permeability and grain size. Groundwater **27**(5), 633–638 (1989)
39. Geldart, D.: Types of gas fluidization. Powder Technol. **7**, 285–292 (1973)
40. Eisfeld, B., Schnitzlein, K.: The influence of confining walls on the pressure drop in packed beds. Chem. Eng. Sci. **56**, 4321–4329 (2001)
41. Gilbertson, M.A., Jessop, D.E., Hogg, A.J.: The effects of gas flow on granular currents. Philos. Trans. R. Soc. A **366**, 2191–2203 (2008)
42. Rao, A., Curtis, J.S., Hancock, B.C., Wassgren, C.: The effect of column diameter and bed height on minimum fluidization velocity. AiChE J. **56**, 2304–2311 (2010)
43. Cheng, N.S.: Wall effect on pressure drop in packed beds. Powder Technol. **210**, 261–266 (2011)
44. Montserrat, S., Tamburrino, A., Roche, O., Niño, Y.: Pore pressure diffusion in defluidizing granular columns. J. Geophys. Res. **117**, F02034 (2012)
45. Mangeney, A., Heinrich, P., Roche, R.: Analytical solution for testing debris avalanche numerical models. Pure Appl. Geophys. **157**, 1081–1096 (2000)
46. Girolami, L., Druitt, T.H., Roche, O.: Towards a quantitative understanding of pyroclastic flows: effects of expansion on the dynamics of laboratory fluidized granular flows. J. Volcanol. Geotherm. Res. **296**, 31–39 (2015)
47. Meruane, C., Tamburrino, A., Roche, O.: On the role of the ambient fluid on gravitational granular flow dynamics. J. Fluid Mech. **648**, 381–404 (2010)
48. Girolami, L., Druitt, T.H., Roche, O., Khrabrykh, Z.: Propagation and hindered settling of laboratory ash flows. J. Geophys. Res. **113**, B02202 (2008)
49. Girolami, L., Roche, O., Druitt, T.H., Corpetti, T.: Velocity fields and depositional processes in laboratory ash flows. Bull. Volcanol. **72**, 747–759 (2010)
50. Iverson, R.M., LaHusen, R.G.: Dynamic pore-pressure fluctuations in rapidly shearing granular materials. Science **246**(4931), 796–799 (1989)